International Journal of Heat and Mass Transfer 54 (2011) 424–432

Contents lists available at ScienceDirect

International Journal of Heat and Mass Transfer

journal homepage: www.elsevier.com/locate/ijhmt

Enhanced heat exchanger design for hydrogen storage using high-pressure metal hydride – Part 2. Experimental results

Milan Visaria, Issam Mudawar *, Timothée Pourpoint

Hydrogen Systems Laboratory, Purdue University, West Lafayette, IN 47907, United States

ARTICLE INFO

Article history:
Received 24 February 2010
Received in revised form 18 August 2010
Accepted 18 August 2010
Available online 11 October 2010

Keywords:
Solid-state hydrogen storage
Heat exchanger
High-pressure metal hydride
$Ti_{1.1}CrMn$

ABSTRACT

Hydrogen storage systems utilizing high-pressure metal hydrides (HPMHs) require a highly effective heat exchanger to remove the large amounts of heat released once the hydrogen is charged into the system. Aside from removing the heat, the heat exchanger must be able to accomplish this task in an acceptably short period of time. A near-term target for this 'fill-time' is less than 5 min. In this two-part study, a new class of heat exchangers is proposed for automobile hydrogen storage systems. The first part discussed the design methodology and a 2-D computational model that was constructed to explore the thermal and kinetic behavior of the metal hydride. This paper discusses the experimental setup and testing of a prototype heat exchanger using $Ti_{1.1}CrMn$ as HPMH storage material. Tests were performed to examine the influence of pressurization profile, coolant flow rate and coolant temperature on metal hydride temperature and reaction rate. The experimental data are compared with predictions of the 2-D model to validate the model, calculate reaction progress and determine fill time. The prototype heat exchanger successfully achieved a fill time of 4 min 40 s with a combination of fast pressurization and low coolant temperature. A parameter termed non-dimensional conductance (*NDC*) is shown to be an effective tool in designing HPMH heat exchangers and estimating fill times achievable with a particular design.

1. Introduction

To achieve a practical mobile onboard hydrogen storage system, high volumetric and gravimetric efficiencies are very important. From a user's point of view, it is equally important that the vehicle can be fueled at the hydrogen station in an acceptably short time. With current state-of-the-art in hydrogen storage using high-pressure metal hydrides (HPMHs), the goal of achieving the DOE fill time of less than 5 min [1] remains quite elusive. The key challenge in achieving this target is tackling the large amounts of heat that are released from the reaction of hydrogen with the HPMH once the hydrogen gas is charged into the vehicle's storage system. This is why the heat exchanger is the most crucial component of a hydrogen storage system utilizing HPMH. But, aside from dissipating the heat, the heat exchanger must be as lightweight as possible and occupy the least volume compared to the metal hydride powder. In this two-part study, an optimized heat exchanger is sought to achieve a fill time of less than 5 min using the HPMH $Ti_{1.1}CrMn$ as hydrogen storage medium. It is important to emphasize, that once the design methodology and associated thermal and kinetic models are demonstrated for this material, it would be easy to extend this technical knowhow to other HPMHs.

The first part of this study [2] discussed both the heat exchanger design methodology and 2-D computational model for a prototype heat exchanger. The heat exchanger was fabricated from aluminum alloy 6061 and occupies 29% of the pressure vessel volume, leaving the remaining volume for the metal hydride. The heat exchanger is 260.3-mm (10.25-in) long and placed inside a 101.6-mm (4-in) diameter pressure vessel for testing. It consists of thin, strategically configured fins that radiate from a coolant U-tube. For $Ti_{1.1}CrMn$, the calculated hydrogen storage capacity is 1.5 wt%, and when activated for testing, it takes the form of fine powder with a particle size of 5–10 μm. Nearly 2.65 kg of the metal hydride powder is packed within cells formed between the heat exchanger fins with an average packing density of 2.5 g/cc. The coolant used is Dex-Cool®, which is a commercial automotive anti-freeze. The 2-D model was based on a coolant temperature of 0 °C and a heat transfer coefficient of 2500 mm^2 K/W. The model predicted that the metal hydride completes 90% of its reaction with hydrogen (hydriding reaction) within 5 min.

Based on this design, the prototype heat exchanger was manufactured for testing and validation of the computational results. This part of this study explores the experimental methods used during the validation tests. The effects of pressurization rate, coolant flow rate, and coolant temperature on the hydriding process are discussed. Metal hydride temperature predictions of the 2-D model are then compared to the measured temperature response of the heat exchanger. Finally, predictions of reaction progress

* Corresponding author. Tel.: +1 (765) 494 5705; fax: +1 (765) 494 0539.
E-mail address: mudawar@ecn.purdue.edu (I. Mudawar).

0017-9310/$ - see front matter © 2010 Elsevier Ltd. All rights reserved.
doi:10.1016/j.ijheatmasstransfer.2010.09.028

Nomenclature

C_a	hydriding constant (s^{-1})
c_p	specific heat (J/kg K)
E_a	activation energy (J/mol of H_2)
F	fraction of completion of reaction
ΔH_r	enthalpy of reaction (J/mol of H_2)
h	convective heat transfer coefficient (W/m^2 K)
k	thermal conductivity (W/m K)
l_{max}	maximum 1-D distance of metal hydride from cooling surface
MW	molecular weight
NDC	non-dimensional conductance
P	pressure (N/m^2)
P_{eq}	equilibrium pressure (N/m^2)
P_o	ambient pressure (N/m^2)
$\dot{q}'''$	volumetric heat generation rate (W/m^3)
R	universal gas constant (8.314 J/mol K)
R_{tc}	contact resistance (mm^2 K/W)
ΔS	entropy of reaction (J/mol of H_2 K)
t	time (s)
T	temperature (K)
$T_{MH,max}$	equilibrium temperature of metal hydride corresponding to maximum hydrogen pressure at end of pressurization ramp
$wt\%$	hydrogen to metal hydride mass ratio when completely hydrided
x	coordinate (mm)
y	coordinate (mm)

Greek symbols

ρ	density
ϕ	porosity

Subscripts

des	desired
eq	equilibrium
f	coolant
in	initial
H_2	hydrogen

are used to determine fill time and identify operating conditions that achieve practical fill times for automobile hydrogen storage systems.

2. Experimental methods

2.1. Hydrogen and coolant flow loops

Fig. 1 shows a simplified schematic diagram of the test facility. The heat exchanger assembly is placed inside a high-pressure vessel. The coolant is supplied at the desired flow rate and temperature from an air-cooled chiller, which is connected to the heat exchanger's coolant U-tube. The chiller is capable of achieving coolant temperatures in the range of 0–25 °C and flow rates as high as 17 lpm. The coolant flows in a closed loop through the heat exchanger and back to the chiller. Not shown in Fig. 1 are several temperature and pressure sensors in the heat exchanger and the pressure vessel that are connected to an instrumentation panel for continuous monitoring and recording of data during the tests.

Hydrogen gas is supplied from hydrogen pressure cylinders containing 5.0-grade hydrogen at 410 bar (6000 psi). The flow of hydrogen to the pressure vessel is controlled by an electronically controlled pressure regulator. A filter helps remove impurities larger than 10 μm from the incoming hydrogen gas cylinders. An on/off valve is used to isolate the heat exchanger from the pressure cylinders. The flow of hydrogen gas into the pressure vessel is measured by a coriolis flow meter. A venturi flow meter is used to measure the hydrogen flow exiting the pressure vessel. Comparing flow rates from the two flow meters helps in detecting and measuring any hydrogen leaks. In addition, three hydrogen sensors placed in the test cell are used to detect any minute hydrogen leaks. All the valves and regulators are remotely actuated from a control room outside the test cell.

During the pressurization, the supply valve is opened and vent valve closed, and the pressure regulator is used to achieve the desired pressurization rate. During the depressurization, the supply valve is closed and vent valve opened. The outflow of hydrogen is controlled by a second regulator in the vent line. The regulator can be programmed to release hydrogen at a rate that simulates the demand of hydrogen gas by a fuel cell onboard a vehicle.

Temperatures of the metal hydride, hydrogen and coolant, pressures, and hydrogen flow rates are continuously monitored and recorded during the tests. Data are analyzed and compared against predictions of the computational model discussed in the first part of this study [2].

2.2. Activation of metal hydride

For the metal hydride to absorb the hydrogen effectively, it must first be activated. Activation is a process of breaking the hydride into small particles to increase surface area, thereby increasing the adsorption and absorption sites for the hydrogen atoms. Activation is achieved by subjecting the metal hydride powder to repeated cycles of high pressure at low temperature, and low pressure (vacuum) at high temperature. The metal hydride powder is first pressurized with 5.0-grade (99.999% purity) hydrogen at 200 bar. During this time, the hydride is placed in a pressure vessel surrounded by a liquid nitrogen bath maintained at −195 °C for 4 h. This is followed by a heating cycle, where the hydride is evacuated to about 0.1 Pa and its temperature raised to 100 °C, during which time a large amount of hydrogen is released. The hydride is then cooled to ambient temperature, completing one activation cycle. This cycle is repeated three times before the hydride is completely activated and ready for testing. At the end of the activation process, metal hydride takes the form of fine powder with particles as small as 5 μm as shown in Fig. 9 in first part of this study [2].

2.3. Heat exchanger assembly in glove box

Fig. 2 shows photos of the sequential stages in preparing the heat exchanger for testing. The activated metal hydride is carefully stored in plastic bags placed within sealed aluminum cans in a glove box where an inert argon atmosphere is maintained with less than 0.1 ppm levels of O_2 and H_2O. Next, all the heat exchanger parts described in the first part of this study [2], including the heat exchanger plates, coolant U-tube, two tapered collets, two cover plates, containment vessel, and instrumentation, are moved into the glove box for assembly and filling. Inside the glove box, the heat exchange plates are combined into stacks of five and the metal hydride powder is filled in the plate cells with a uniform packing density of 2.5 g/cc. Two of the plates support stainless posts that hold thermocouples at precise locations within the metal hydride. The filled plates are loosely mounted on the collets and the coolant tube is slid through the collets. The loose assembly is then

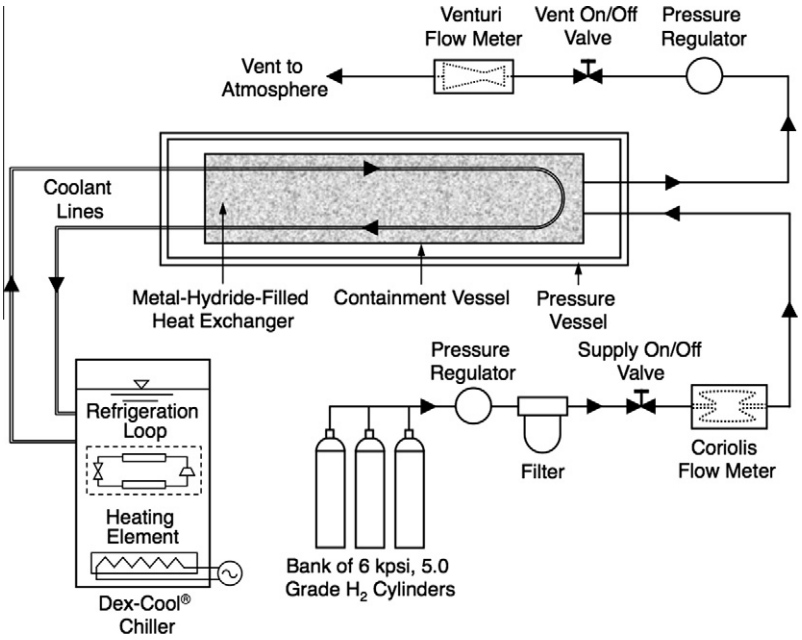

Fig. 1. Schematic diagram of test facility.

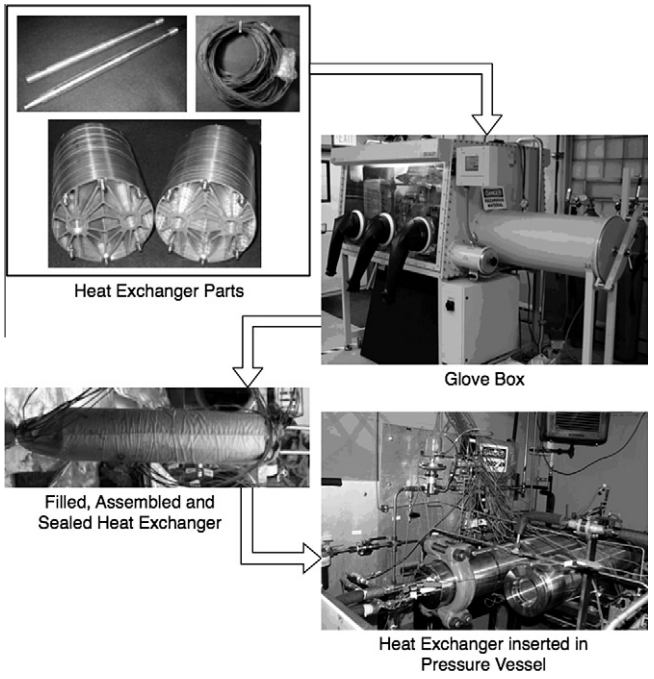

Fig. 2. Photos depicting sequential stages of heat exchanger preparation for testing.

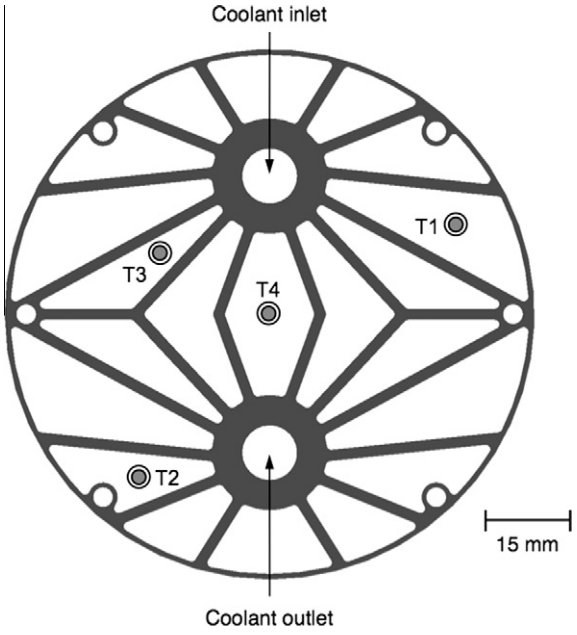

Fig. 3. Thermocouple locations.

tightened together with the aid of two pairs of hexagonal nuts on the ends of the collets and six pairs of nuts on the threaded rods that run through the entire assembly. This locks the heat exchanger components in place and eliminates any gaps between adjacent plates that may arise from minute surface imperfections. The cover plates and thin-walled containment vessel provide the required sealing and restrict the metal hydride powder from leaking out of the cells. The final attachments to the heat exchanger assembly are the two check valves and the two coolant tube fittings. The assembly is then covered with an insulating Nylon casing and is ready for transport from the glove box to the pressure vessel for testing.

2.4. Assembly in the pressure vessel

Utmost care is taken to avoid any metal hydride exposure to air or moisture as the assembled heat exchanger is transported from the glove box to the pressure vessel. During the transit, all the in/out ports on the heat exchanger are sealed. The pressure vessel is made from 304 stainless steel and certified for 410 bar (6000 psi). Once the heat exchanger assembly is inserted into the pressure vessel, all pressure and temperature sensors as well as connections to the hydrogen and coolant flow lines are secured. After sealing the pressure vessel and securing all the connections, the heat exchanger is ready for testing.

When the heat exchanger is not being tested, a positive hydrogen pressure of 7 bar is maintained at all times in the pressure

vessel to ensure that, in the event of even a minute leak, air would never enter the pressure vessel.

2.5. Temperature measurements

Temperatures are measured using four type-T thermocouples placed within the metal hydride powder. 0.13-mm diameter thermocouple wire is used to achieve fast temperature response. The temperature measurements are made in planes 1/4 and 3/4 along the length of the heat exchanger. As shown in Fig. 3, thermocouple locations are chosen to help understand the effects of cell size and proximity to the coolant tube and fin surfaces on hydride temperature. Thermocouples T1 and T4 are located near the centers of larger cells, while thermocouples T2 and T3 are located in smaller cells close to fin surfaces.

2.6. Test matrix

Table 1 shows a summary of the five tests that were performed to assess the performance of the prototype heat exchanger. These tests include variations in pressurization rate, maximum hydriding pressure, coolant flow rate and temperature, and initial metal hydride temperature. Maximum hydriding pressures of 280 and 330 bar, and three different pressurization rates are examined. In tests A, B and D, the pressure during hydriding is increased linearly from 70 to 280 bar in 60 s. In test C, the pressurization rate is the fastest, increasing from 7 to 330 bar in 60 s, while it is slowest in test E, increasing from 70 to 280 bar in 300 s. These experiments show how various parameters affect hydriding rate and the conditions under which desired fill times can be achieved. Coolant flow rates and temperatures of 17 and 1.7 lpm and 0 and 20 °C, respectively, are examined. In test B, no coolant is supplied through the U-tube. The initial temperature of the metal hydride is varied between 0.5 and 17 °C.

3. Experimental results

3.1. Testing cycle and measured profiles

The data for test D are presented first to explain the hydrogen flow rate and metal hydride temperature profiles during a complete cycle in response to the pressurization profile. For uniformity and ease of comparison with data from other tests, the time axis for all plots hereafter have been shifted so that the start of the pressurization ramp is indicated as zero reference time.

Fig. 4 shows the hydrogen flow rates profiles during the pressurization and venting out of the pressure vessel. Before a test, all the primary test parameters such as coolant temperature, coolant flow rate and the hydriding pressurization profile are established. Next, extensive safety checks are performed. This is followed by setting the coolant temperature and flow rate to the desired levels. While the coolant achieves the set temperature, manual leak checks are performed. Notice there are three spikes in the inlet hydrogen flow rate prior to the pressurization ramp. The first spike is observed when the pressure is increased from

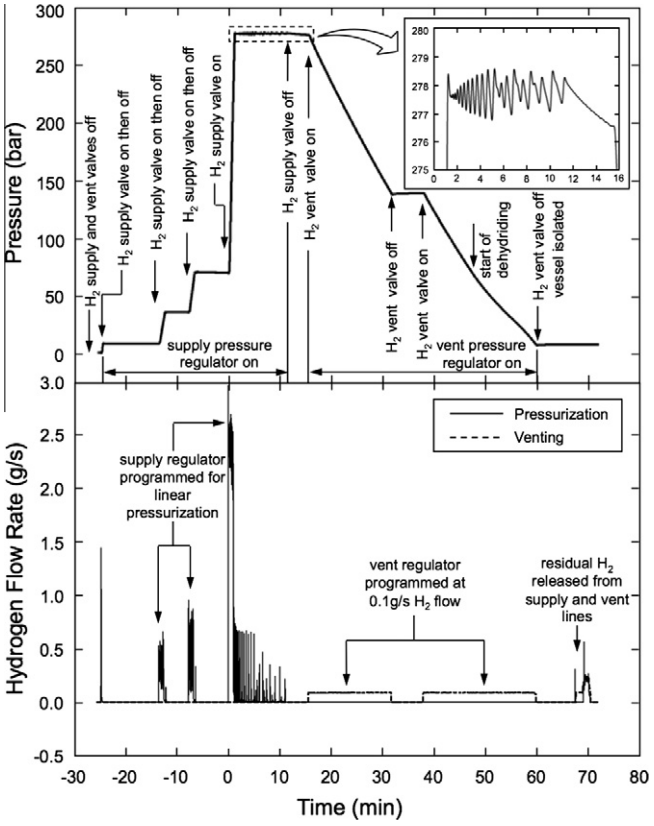

Fig. 4. Pressure and flow rate profiles from test D.

atmospheric to 7 bar, the second to 35 bar and the third to 70 bar. During the pressurization, the hydrogen outlet valve is closed and, hence, no flow is measured by the flow meter in the vent line. Upon reaching 35 bar and later 70 bar, the inlet valve is closed to isolate the pressure vessel and check for leaks. Manual leak checks of all fittings on the pressure vessel as well as the hydrogen and coolant lines are performed. If any leak is detected, the tank is depressurized and the leak fixed. If the system is free from leaks at 35 bar, the pressure is increased to 70 bar and the system checked for leaks once more. This is the maximum pressure at which manual leak checks are performed. Operators are restricted from entering the test cell above this pressure, and thereafter all testing is resumed remotely from the adjoining control room. Above 70 bar, any hydrogen leak in the system is detected with the aid of three hydrogen sensors in the test cell and also the pressure sensors at various locations within the flow loop, since any unexpected drop in pressure within the pressure vessel or hydrogen lines may be an indication of a leak. Flat pressure plateaus at these two pressures indicate the absence of any leaks. After the coolant reaches the desired flow rate and temperature, and the leak checks completed, pressurization is initiated. Pressurization rates as high as 1–330 bar in 30 s can be achieved. In this test, the inlet valve is opened again for 60 s and the pressure is

Table 1
Summary of tests performed.

Test no.	Pressurization profile	Coolant flow rate	Coolant temp. (°C)	Initial temp. (°C)	Major objectives
A	70–280 bar in 60 s	171 pm (4.5 gpm)	20	17	Effect of coolant temperature
B	70–280 bar in 60 s	No coolant		16	Effect of heat exchanger
C	7–330 bar in 60 s	171 pm (4.5 gpm)	0	0.5	Effect of fast pressurization
D	70–280 bar in 60 s	1.71 pm (0.45 gpm)	0	4	Effect of low coolant flow rate
E	70–280 bar in 300 s	171 pm (4.5 gpm)	0	5.4	Effect of slow pressurization

linearly increased from 70 to 280 bar. A hydrogen flow rate up to 3 g/s is measured during a minute-long pressurization ramp. Once the pressure reaches 280 bar, the inlet valve is kept open to maintain constant pressure during hydriding. The pressure regulator ensures that, if the pressure decreases by more than one bar due to hydriding or cooling, hydrogen is pumped into the pressure vessel. This can be seen in the inset in Fig. 4, which shows the pressure profile during the hydriding reaction. As the hydride reacts with hydrogen, the pressure decreases due to the hydriding, prompting the pressure regulator to allow more hydrogen into the vessel, thereby increasing the pressure. The process is manifest in the form of a pressure fluctuation whose magnitude increases but frequency decreases with time indicating a decreasing rate of hydriding reaction. This can also be verified from the plot of hydrogen flow rate where, after the end of the pressurization ramp, the rate of hydrogen flow rate gradually subsides. The rate of hydriding is at its peak during the pressurization ramp and for a couple of minutes thereafter. It can be seen from the pressure profile during hydriding that, at the end of 7 min, the frequency of pressure fluctuations significantly subsides, indicating that most of the hydriding reaction is complete. Once the hydriding is fully complete at 7 min, the inlet valve is closed a little later (at 10 min) and the pressure vessel is isolated. The outlet valve is then opened to initiate the dehydriding process. The pressure vessel is depressurized at a very slow rate by venting the hydrogen gas at 0.1 g/s. Initially, the decrease in pressure is the result of venting of the hydrogen gas stored in the empty spaces of the pressure vessel and in the gaps between metal hydride particles. Dehydriding does not occur until after 45 min when the pressure reaches about 70 bar, where a slight change in the slope of the pressure curve can be seen. This slope change is caused by a drop in the rate of pressure decrease as hydrogen begins to be released by the dehydriding process. When the dehydriding process ends, the pressure vessel is isolated and the metal hydride is stored at 7 bar.

Fig. 5 shows metal hydride temperature profiles measured by thermocouples T1–T4 along with mean coolant temperature (average of coolant's inlet and outlet temperatures) from test D. Any small rise in the pressure is accompanied by a small increase in metal hydride temperature. This is due to pressurization heating. The pressurization ramp from 70 to 280 bar is accompanied by a steep rise in temperature from about 2 °C to a maximum of 50 °C within 60 s. The coolant temperature rises by a maximum of 1.5 °C during hydriding due to the heat removed from the metal hydride. The rise in the hydride temperature is the result of the heat released due to both hydriding and pressurization. The slope of this temperature rise depends on the properties of the metal hydride; this slope is identical for all four thermocouples. The equilibrium temperature corresponding to 280 bar is 50 °C and, hence, the metal hydride temperature does not exceed 50 °C at any location. Should the temperature at a given location rise to equilibrium, the reaction would stop and then continue only after the metal hydride cools down below equilibrium. Notice that thermocouple T4 measured the highest temperature rise while T1 measured the lowest. Temperatures at locations other than T4 never reached 50 °C, indicating higher heat transfer rates at these locations. It is obvious why T2 and T3, which both measured maximum temperatures of 48 °C, correspond to locations that provide better cooling than that for T4. Both are situated in relatively narrow cells close to fin surfaces compared to T4. However, it is not obvious why T1, which measured a maximum temperature of only 38 °C, would correspond to a more favorable cooling location than the other three thermocouples, given that it is located in a relatively large cell and a bit more remote from fin surfaces. Interestingly, T1 showed lowest measurements in all other four tests as well. This behavior can be explained by the packing of metal hydride powder around the thermocouple probe. During the packing, it is possible

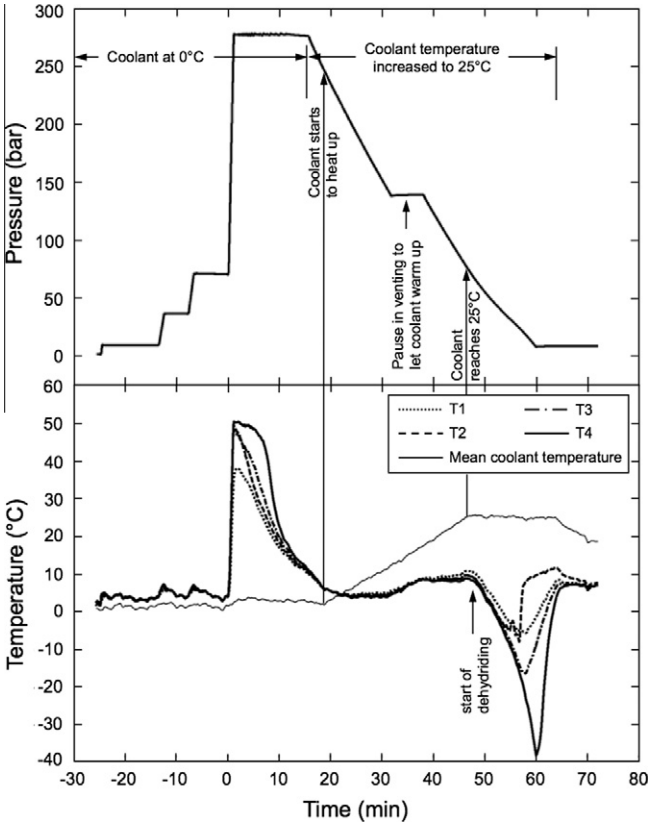

Fig. 5. Pressure and temperature profiles from test D.

that either the hydride powder did not have good contact with the thermocouple bead or that low hydride powder density around the thermocouple bead caused a localized decrease in the hydride temperature during hydriding. Additionally, any slight movement of powder as a result of repeated expansion and contraction between tests could contribute to inconsistent or low powder densities around a particular thermocouple.

Located in small cells close to both fin surfaces and coolant tubes, thermocouples T2 and T3 measured the fastest cooling rates. They measured peak temperatures at the end of the pressurization ramp but dropped rapidly immediately afterwards. This shows heat removal rates at T2 and T3 were very high compared to heat generation due to hydriding. Hydriding reactions in these smaller cells were completed at least 1.5–2 min before the larger cells. This supports the use of the maximum hydride layer thickness criterion for heat exchanger design and for achieving a particular fill time as discussed in the first part of this study [3]. Thermocouple T4 is located in the largest cell midway between the coolant inlet and outlet tubes. Among all the thermocouples, T4 measured the highest temperatures in all the tests. Following the completion of the pressurization ramp, the metal hydride temperature measured by T4 dropped by only 5 °C in about 7 min. This implied that heat removal at this location is far less effective than at the locations of T2 and T3. However, after 7 min, the hydriding reaction at T4 was complete and the temperature dropped sharply, by more than 25 °C in 3 min. Finally, the metal hydride in all the heat exchanger cells reached uniform temperature.

For dehydriding, the inlet hydrogen valve was closed and the outlet opened to vent the hydrogen. At the same time, the coolant temperature was set to 25 °C. Initially, when the hydrogen was vented from the pressure vessel, the metal hydride temperature decreased due to depressurization. Thereafter, as the pressure decreased further, the hydride temperature increases because of the

increasing coolant temperature. At about 70 bar, the dehydriding commenced and was accompanied by a sharp decrease in the metal hydride temperatures. There appears to be a correspondence between the temperature drop during the dehydriding and the temperature rise during the hydriding. For example, thermocouple T4, which measured the highest temperature of 50 °C during hydriding, also measured the lowest temperature of −38 °C during dehydriding. This large temperature drop is the result of the large heat of reaction (−22 kJ/mol of H_2 [4]) associated with the endothermic dehydriding reaction. The extent of temperature drop also depends on the rate of hydrogen release, which is 0.1 g/s for the present study. Lower temperatures are possible by increasing the hydrogen release rate. Once the metal hydride is completely dehydrided, its temperature increases again and quickly reaches ambient temperature.

3.2. Hydriding temperature profiles

The present work is focused on the hydriding reaction and means to maximize reaction rate. Hence, hereafter, only the data obtained during the hydriding period of the testing cycle are discussed and later compared with the results of the computational model. Fig. 6 shows the pressure and hydriding temperature profiles for test A, in which the coolant was set at a flow rate of 17 lpm (4.5 gpm) and 20 °C, the highest temperature of all five tests. Before the start of pressurization, the metal hydride was at 17 °C, which corresponds to an equilibrium pressure of 150 bar. Hence, it took a few seconds before the pressure exceeded 150 bar and the hydriding began. Until then, the temperature rise was due to pressurization heating. Hydriding can be detected from the increase in slope of the temperature profile around 150 bar.

This increase in slope and start of the hydriding is even more pronounced for the temperature profiles for test E as shown in Fig. 7. Unlike all the other tests, where the pressure ramp took only 60 s, the pressure in test E was increased from 70 to 280 bar in 5 min. The coolant temperature in test E was 0 °C compared to 20 °C in test A, while the flow rate was the same for both tests at 17 lpm (4.5 gpm). In both tests, T4 measured the same peak temperature of 50 °C. Other thermocouples measured 3–5 °C lower in test E compared to those in test A. This is because of the lower coolant temperature and slower pressurization rate in test E. Although the coolant temperature and pressurization rate are different for the two tests, the time it took to complete the hydriding reaction is about the same. For test A, where the coolant temperature is higher and the pressurization rate faster, the hydriding reaction is thermally limited. In this case, the hydriding rate could benefit from a faster cooling rate, such as lowering the coolant temperature. On the other hand, for test E, a slow pressurization rate implies that the hydriding reaction is kinetically limited. In other words, the cooling rate provided by the heat exchanger is sufficient for test E, but the pressure is not much above the equilibrium pressure to accelerate the reaction. In general, the hydriding reaction is thermally limited if the metal hydride temperature stays near its peak value for a long time due to an insufficient cooling rate. On the other hand, the hydriding reaction may be kinetically limited if the metal hydride temperature drops quickly as soon as the pressurization ends.

Fig. 8 compares temperature profiles measured by thermocouple T4 from tests B and C. In test B, no liquid coolant was used and the metal hydride was cooled by free convection from the ambient air outside the pressure vessel. In test C, the pressurization rate was highest, increased from 7 to 310 bar in 60 s, compared to 70 to 280 bar in 60 s for test B. The coolant flow rate for test C was also highest at 19 lpm (4.5 gpm) and coolant temperature lowest, 0 °C. These conditions increased the kinetic and as well as thermal limit for test B, resulting in faster hydriding rates. Com-

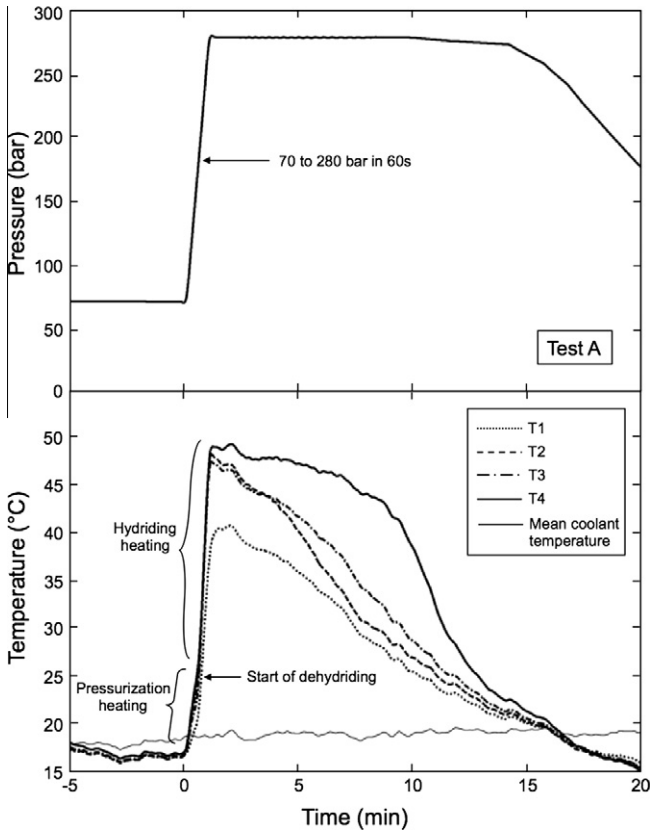

Fig. 6. Pressure and temperature profiles from high coolant temperature test (A).

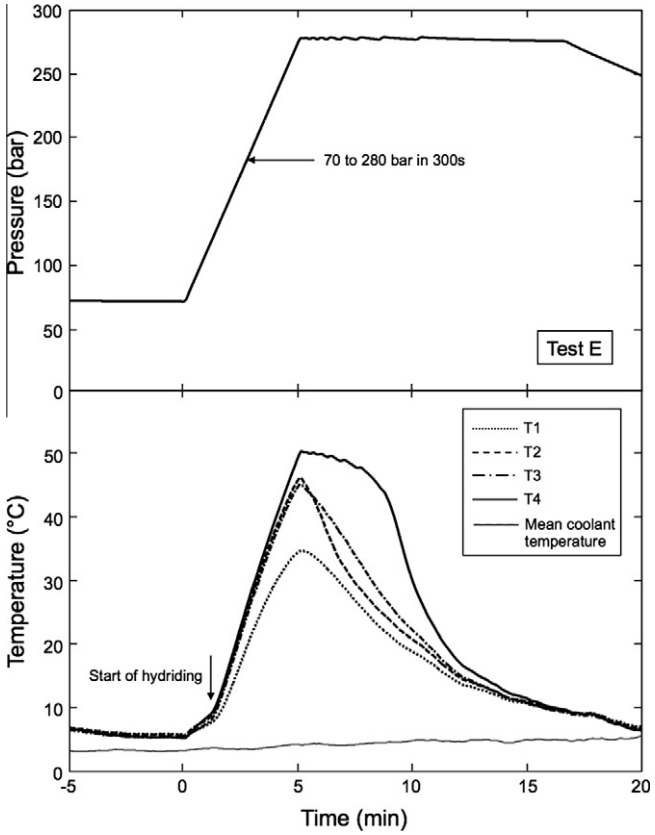

Fig. 7. Pressure and temperature profiles from slow pressurization test (E).

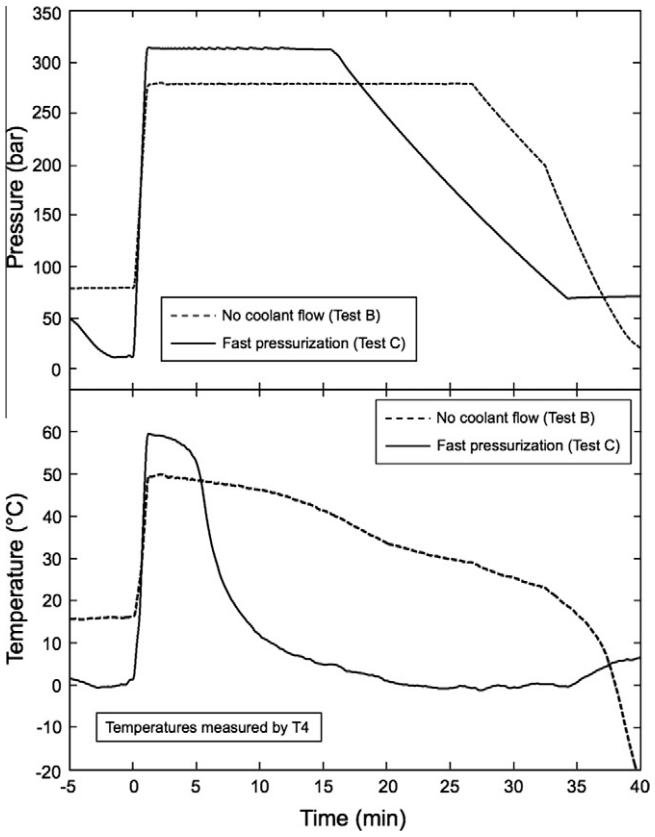

Fig. 8. Comparison of pressure and temperature profiles from tests B and C.

paring tests B and C provides a basis for evaluating of the improvement resulting from the use of an optimized heat exchanger in a HPMH hydrogen storage system. In absence of liquid coolant, the initial hydride temperature for test B is higher than that for test C, 16 versus 0.5 °C. Also, the peak temperature measured by T4 in test C is 60 °C, which is the equilibrium temperature at 310 bar, while in test B the peak temperature is 50 °C, the equilibrium value at 280 bar. The differences in reaction rate and fill time between the two tests are readily manifest from the two temperature profiles. Though peak temperature for test C is 10 °C higher, it drops much faster. The temperature drop is quite steep once the hydriding is complete, by 25 °C in less than 2 min. By comparison, it takes for the metal hydride in test B more than 15 min to cool down from 50 to 40 °C. Furthermore, hydriding in test B reaches the thermal limit due to insufficient cooling, relying only on free convection from ambient air outside the pressure vessel to cool the metal hydride. This results in poor hydriding rates and causing fill time to be three to four time longer that for test C. This shows how it is virtually impossible to meet the 5 min fill time requirement of automobiles without an optimized heat exchanger.

4. Comparison with computational model predictions and calculation of fill time

4.1. Computational model

A 2-D computational model was constructed in Fluent to determine the temperature of the metal hydride during the hydriding phase, and also to calculate the fill time. Fill time is defined as the time required for the metal hydride to complete 90% of the reaction. Complete details of the model can be found in the first part of this study [2]. The temperature of metal hydride is calculated by solving the 2-D heat diffusion equation in response to heat generated by both the reaction and the pressurization

$$\dot{q}''' = \frac{dF}{dt}\frac{(wt\%)\rho_{MH}}{MW_{H_2}}\Delta H_r + \phi\frac{dP}{dt}. \quad (1)$$

Assuming 1st order kinetics, the heat generation due to the reaction of hydrogen with the metal hydride is given by [5,6]

$$\frac{dF}{dt} = C_a \exp\left(\frac{-E_a}{RT}\right)\ln\left(\frac{P}{P_{eq}}\right)(1-F), \quad (2)$$

where F is the fraction of completion of reaction. P_{eq} is the equilibrium pressure that depends on the metal hydride temperature and kinetic properties and is given by the van't Hoff equation

$$P_{eq} = P_o \exp\left(\frac{\Delta H_r}{RT} - \frac{\Delta S}{R}\right). \quad (3)$$

The energy and kinetics equations are solved simultaneously to determine $T(x, y, t)$ and $F(x, y, t)$. Temperatures are then compared to the profiles measured at the four thermocouple locations. The fraction of reaction completion, F, is averaged over the entire cross-section of the heat exchanger and fill time is defined as the time corresponding to $F = 0.9$.

Table 2 lists the metal hydride properties and coolant conditions used in the model. Using Eq. (3) for equilibrium pressure, and the variation of temperature with pressure during pressurization, the enthalpy of reaction and entropy of reaction are calculated and reconfirmed as $\Delta H_r = -14{,}390$ J/mole-H_2 and $\Delta S = -91.3$ J/mol of H_2, respectively. Values of the other kinetic and thermal parameters in Table 2 are obtained either from the literature [7–9] or measured at the Purdue Hydrogen Systems Laboratory [10] (further details can also be found in part 1 of this study [2]). When comparing the computational model predictions with experimental data, all kinetic and thermal properties are held constant for a given test. The only parameters that are varied in the model are pressurization profile, coolant flow rate and coolant temperature, which match the operating conditions of the particular test being modeled.

4.2. Comparison with model predictions

Figs. 9 and 10 compare the experimental data and computational model predictions for thermocouple T4. They also show calculated reaction progress (fraction of reaction completion) for the same tests. Fig. 9 compares results for tests C and E, which involve the same coolant temperature of 0 °C. The initial metal hydride temperature for test E is 5.4 °C, 5 °C higher than for test C. But the main difference between the two tests is a much faster pressurization rate for test C, 7–310 bar in 60 s, compared to that for test E,

Table 2
Metal hydride properties and coolant conditions used in model.

Kinetic	
Activation energy	$E_a = 20.7$ kJ/mol H_2
Enthalpy of formation	$\Delta H_r = -14{,}390$ J/mol H_2
Entropy of formation	$\Delta S = -91.3$ J/mol H_2
Activation rate	$C_a = 150\ s^{-1}$
H_2 storage capacity	1.5 wt%
Thermal	
Packing density	$\rho_{MH} = 2500$ kg/m^3
Effective thermal conductivity	$k_{MH} = 1$ W/m K
Specific heat	$c_{pMH} = 500$ J/kg K
Contact resistance	$R_{tc} = 2000$ mm^2 K/W
Coolant	
Temperature	$T_f = 0$ or 20 °C
Convection coefficient	$h_f = 1500, 2500$ W/m^2 K

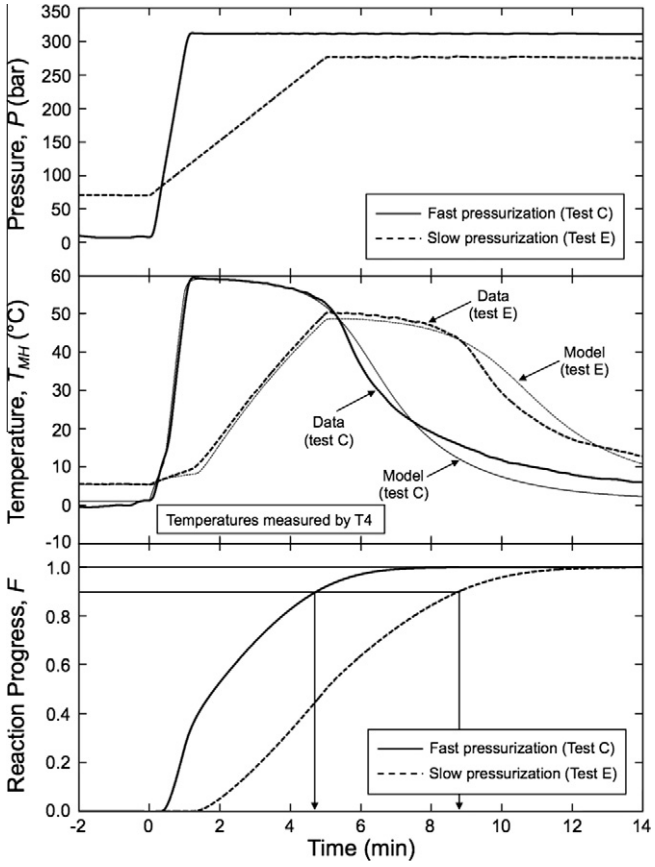

Fig. 9. Comparison of data and computational model predictions for tests C and E.

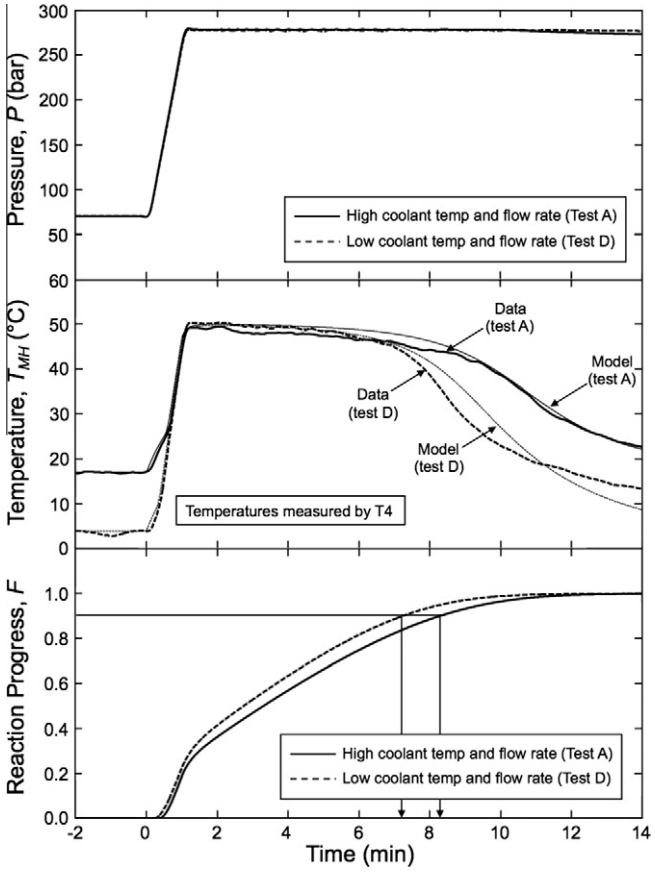

Fig. 10. Comparison of data and computational model predictions for tests A and D.

70–280 bar in 300 s. Fig. 9 shows excellent agreement between measured and predicted temperature profiles for both tests, especially during hydriding. In the model, which primarily predicts the process of hydriding, a maximum deviation of 1.7 °C is observed between the measured and predicted values for both tests in the hydriding phase. This corresponds to less than 4% of the ΔT_f, difference between the temperature measured by T4 and the coolant temperature. A discrepancy between the measured and predicted temperatures is observed only once the hydriding process is completed. A maximum deviation of 6.5 °C (or 20% of ΔT_f) is observed in test E, way past the fill time. The main reason for the deviation between the temperatures following the completion of the hydriding is the assumption of constant metal hydride properties in the model. In reality, the properties of the metal hydride, especially k_{MH} and $c_{p,MH}$, will vary with hydrogen content and the variation is more pronounced towards the end of the hydriding process [10]. Plotted in the same figure is the average reaction progress for the entire duration of hydriding in each test. Recall that the fill time is calculated as the time required to complete 90% of the reaction, which corresponds to 4 min 40 s for test C versus 8 min 30 s for test E. Therefore, test C was successful at meeting the 5 min fill time. Lower peak pressure and slower pressurization rate in test E provided smaller driving force for hydriding, resulting in a longer fill time compared to test C. From the plot of reaction progress, it can be seen that it takes some time before the reaction is initiated. For test C, no reaction occurs during the first 25 s following the onset of pressurization while, for test E, slow pressurization prolongs this initial period to 1.5 min. In both tests, reaction rate is highest in the initial stages after which it continuously slows down because of the self-limiting nature of the reaction. For test C, it takes only 1 min to complete the first 30% of the hydriding reaction. However, after finishing 90% of the reaction, it takes many minutes to complete the final 10% of the reaction. This is why it is impractical to wait for the entire hydride to finish the reaction, and fill time is based on 90% rather than 100% of completion of the hydriding reaction.

Fig. 10 shows a similar plot for tests A and D. Both tests have exactly the same pressurization rate from 70 to 280 bar in 60 s. Test A has a high coolant flow rate of 17 lpm (4.5 gpm) at 20 °C, while test D has one-tenth the flow rate and a lower temperature of 0 °C. A good agreement between the experimental data and model results can be seen in this plot as well. The largest deviation between the measured and predicted temperature during the hydriding phase is only 3 °C, which is 8% of ΔT_f. Following the completion of the hydriding, the maximum deviation is 6 °C (21% of ΔT_f) for test D. The model calculates a fill time of 8 min 15 s for test A, about a minute longer than test D. Though the pressurization rate is the same, the lower coolant temperature in test D causes the metal hydride to react faster compared to test A. Heat transfer rate is lower with a lower coolant flow rate but the effect of coolant flow rate is less pronounced compared to that of coolant temperature. In [3], it was showed that coolant temperature had a greater impact on reaction rate than coolant flow rate and above a certain value, increasing the coolant flow rate does not yield any appreciable improvement in reaction rate.

4.3. Results summary

In a previous work by the authors [3], a parameter termed nondimensional conductance (*NDC*) was developed to investigate the effects of various HPMH heat exchanger parameters and their relative importance on fill time. *NDC* is defined as the ratio of the maximum heat rate that can be removed from the metal hydride

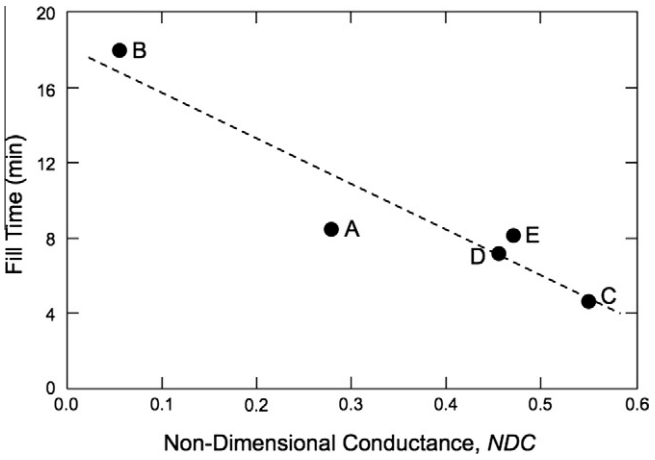

Fig. 11. Variation of fill time predicted from computational model for five tests with non-dimensional conductance.

under a prescribed set of operating conditions to the heat rate that could be generated for a specified thickness of metal hydride to react completely in the desired time

$$NDC = \frac{\left(\frac{T_{MH,max}-T_f}{\frac{1}{h_f}+R_{tc}+\frac{l_{max}}{k_{MH}}}\right)}{\left(\frac{\Delta H_r (wt\%)\rho_{MH}}{MW_{H_2}}\frac{l_{max}}{t_{des}}\right)}, \quad (4)$$

where t_{des} is the desired fill time and l_{max} is the maximum 1-D distance of metal hydride from a cooling (fin) surface. The *NDC* is a measure of the fraction of heat generation rate due to hydriding that can be removed by the heat exchanger. A higher *NDC* amounts to higher heat transfer rates. $T_{MH,max}$ in Eq. (4) is the equilibrium temperature of the metal hydride corresponding to the maximum hydrogen pressure at the end of the pressure ramp.

Fig. 11 shows fill times calculated from the Fluent models for all five tests plotted against *NDC*. As expected, the plot shows a trend of decreasing fill time with increasing *NDC*. Of all the tests, *NDC* is highest for test C and smallest for test B. With its fastest pressurization rate, test C also achieved the lowest fill time of 4 min 40 s, while, in the absence of coolant, test B yielded the longest fill time of 18 min. The fill times and *NDC* values for tests A (high coolant temperature), D (low coolant flow rate) and E (slow pressurization rate) lie between the corresponding values for tests B and C. Fig. 11 proves *NDC* is a very useful parameter for designing HPMH heat exchangers and estimating fill times achievable with a particular heat exchanger design.

5. Conclusions

In this second part of a two-part study, experiments were performed with a prototype heat exchanger filled with high-pressure metal hydride (HPMH) to achieve a fill time of less than 5 min for automobile hydrogen storage applications. Five tests were performed to examine the influence of pressurization profile, coolant flow rate and coolant temperature on the hydriding reaction and fill time. The experimental data were then compared with predictions of a 2-D computational model. Key findings from the study are as follows.

1. During the hydriding phase, metal hydride in smaller heat exchanger cells and closer to fin surfaces achieves lower temperatures and higher cooling rates, while metal hydride in the interior of larger cells achieves higher peak temperatures and takes longer to finish hydriding.
2. Peak temperature of the metal hydride is limited by equilibrium temperature corresponding to the hydrogen pressure. Once this temperature is reached, the metal hydride stops reacting until it is cooled below the equilibrium temperature. Completion of the hydriding reaction is accompanied by a rapid drop in the metal hydride temperature.
3. The prototype heat exchanger successfully achieved the fill time of less than 5 min. The shortest fill time of 4 min 40 s was achieved with the fastest pressurization rate and lowest coolant temperature, while, absent coolant flow, fill time was longest, exceeding 18 min. This highlights the crucial role of the heat exchanger in a HPMH storage system. Although, providing such high cooling rates may seem restrictive, it must be remembered that cooling is required only during the charging (filling) of hydrogen into the metal hydride and hence the coolant system can be located at the filling station and need not be onboard the vehicle.
4. A parameter termed non-dimensional conductance (*NDC*), that was previously developed by the authors as a measure of the fraction of heat generation due to hydriding that can be removed by the heat exchanger, is shown to be very effective in designing HPMH heat exchangers and estimating fill times achievable with a particular design.

Acknowledgement

This study was partially supported by General Motors Corporation.

References

[1] DOE, Hydrogen, fuel cells and infrastructure technologies program, multi-year research, development and demonstration plan: planned program activities for 2005–2015, Energy Efficiency and Renewable Energy, US Department of Energy, Washington, DC, 2007.
[2] M. Visaria, I. Mudawar, T. Pourpoint, Enhanced heat exchanger design for hydrogen storage using high-pressure metal hydride – Part 1. Design methodology and computational results, Int. J. Heat Mass Transfer 54 (2011) 413–423.
[3] M. Visaria, I. Mudawar, T. Pourpoint, S. Kumar, Parametric study of heat transfer and kinetics parameters influencing the design of heat exchangers for hydrogen storage in high-pressure metal hydrides, Int. J. Heat Mass Transfer 53 (2010) 2229–2239.
[4] Y. Kojima, Y. Kawai, S. Towata, T. Matsunaga, T. Shinozawa, M. Kimbara, Development of metal hydride with high dissociation pressure, J. Alloys Compd. 419 (2006) 256–261.
[5] U. Mayer, M. Groll, W. Supper, Heat and mass transfer in metal hydride reaction beds: experimental and theoretical results, J. Less-Common Metals 131 (1987) 235–244.
[6] A. Jemni, S. Ben Nasrallah, Study of two-dimensional heat and mass transfer during absorption in a metal-hydrogen reactor, Int. J. Hydrogen Energy 20 (1995) 43–52.
[7] S. Suda, Y. Komazaki, N. Kobayashi, Effective thermal conductivity of metal hydride beds, J. Less-Common Metals 89 (1983) 317–324.
[8] D. Dedrick, M.P. Kanouff, B.C. Replogle, K.J. Gross, Thermal properties characterization of sodium alanates, J. Alloys Compd. 389 (2005) 299–305.
[9] S. Suda, N. Kobayashi, K. Yoshida, Reaction kinetics of metal hydrides and their mixtures, J. Less-Common Metals 73 (1980) 119–126.
[10] S. Flueckiger, T. Voskuilen, T. Pourpoint, T.S. Fisher, Y. Zheng, In situ characterization of metal hydride thermal transport properties, Int. J. Hydrogen Energy 35 (2010) 614–621.